Scanning electron microscope imaging of grain structure and phase distribution within gas-hydrate-bearing intervals from JAPEX/JNOC/GSC et al. Mallik 5L-38: what can we learn from comparisons with laboratory-synthesized samples?

L.A. Stern[1], S.H. Kirby[1], and W.B. Durham[2]

Stern, L.A., Kirby, S.H., and Durham, W.B., 2005: Scanning electron microscope imaging of grain structure and phase distribution within gas-hydrate-bearing intervals from JAPEX/JNOC/GSC et al. Mallik 5L-38: what can we learn from comparisons with laboratory-synthesized samples?; in *Scientific Results from the Mallik 2002 Gas Hydrate Production Research Well Program, Mackenzie Delta, Northwest Territories, Canada, (ed.) S.R. Dallimore and T.S. Collett; Geological Survey of Canada, Bulletin 585, 19 p.*

Abstract: Cryogenic scanning electron microscopy provides an excellent means for examining phase distributions, grain morphologies, and grain contacts within gas-hydrate-bearing samples of both natural and laboratory origin. Here, recovered samples from JAPEX/JNOC/GSC et al. Mallik 5L-38 are imaged, and comparisons are made between the geometrical arrangement and appearance of the gas hydrate ± ice phase and arrangements, grain contacts, and textures displayed by pure gas hydrate and gas hydrate–sediment aggregates grown and tested in the laboratory. Many gas hydrate ± ice sections in Mallik samples occur as smooth, dense material surrounding isolated macropores, whereas other closely juxtaposed sections display highly mesoporous textures. The possible origins of the mesoporosity are evaluated, and likewise the origin of ice mixed with the gas hydrate, both of which influence interpretations of physical-property measurements. Lastly, the authors image lab-synthesized methane hydrate+quartz aggregates using phase proportions comparable to those displayed by Mallik material from sand intervals, and discuss the implications of strength measurements made on the synthetic samples.

Résumé : La microscopie électronique à balayage avec platine cryogénique est une excellente méthode pour examiner la répartition des phases, la morphologie des grains et la nature des joints intergranulaires dans des échantillons naturels ou synthétiques renfermant des hydrates de gaz. Au moyen de cette technique, nous avons obtenu des images d'échantillons prélevés dans le puits de recherche sur la production d'hydrates de gaz JAPEX/JNOC/GSC et al. Mallik 5L-38, et nous avons comparé les agencements géométriques, les joints intergranulaires et les textures de la phase hydrates de gaz ± glace dans ces échantillons à ces caractéristiques dans des échantillons produits et éprouvés en laboratoire, constitués soit d'hydrates de gaz purs ou d'agrégats d'hydrates de gaz et de sédiments. Dans un grand nombre des tranches d'échantillons provenant du puits Mallik, la phase hydrates de gaz ± glace montre une texture dense et unie avec des macropores isolés, alors que dans des tranches voisines cette phase a une texture fortement mésoporeuse. Nous avons considéré les origines possibles des mésopores et celles de la glace mêlée aux hydrates de gaz, deux facteurs qui influencent l'interprétation des mesures de propriétés physiques. Nous avons également obtenu des images d'agrégats synthétiques contenant de l'hydrate de méthane et du quartz en proportions comparables à celles des échantillons prélevés dans des intervalles de sable du puits Mallik. De plus, nous discutons des implications de mesures de résistance effectuées sur les échantillons synthétiques.

[1]United States Geological Survey, 345 Middlefield Road, MS/ 977, Menlo Park, California 94025 U.S.A.
[2]U.C. Lawrence Livermore National Laboratory, P.O. Box 808, Livermore, California 94550 U.S.A.

INTRODUCTION AND BACKGROUND

One of the challenges of investigating both natural and laboratory-made gas hydrate involves careful evaluation of their grain and pore structures, characteristics that can be useful guides to in situ initial growth conditions as well as to the effects of changes in environmental conditions including those during recovery, handling, transport, and/or storage. The amount, geometrical distribution, fabric, and morphologies of gas hydrate in nature not only influence properties of sediments or formations in which they occur, but can also affect physical-property measurements made on recovered samples.

Scanning electron microscopy (SEM) offers significant potential for obtaining such textural information due to its versatility in detection capabilities, its potential resolution, and its large depth of focus. When applied to gas hydrate, however, there are a number of technical challenges: avoiding condensation of atmospheric water on samples during cold transfer, maintaining the gas hydrate sample material at conditions that avoid spontaneous decomposition or significant sublimation under vacuum, and either avoiding electron beam damage of the imaging area or learning to properly identify it when it does occur. Distinguishing handling-induced surface artifacts from the intrinsic sample surface morphology can also be difficult, as well as distinguishing gas hydrate from ice.

Use of SEM for imaging gas hydrate has only recently been reported in the literature. W. Kuhs, D. Staykova, A. Klapproth, G. Genov, and coworkers (Kuhs et al., 2000; Staykova et al., 2003; Klapproth et al., 2003; Genov et al., 2004) used SEM techniques with excellent success in imaging and identifying grain structures in CH_4, CH_4-N_2, CO_2, and Ar hydrate prepared from reaction of ice with gases or liquids, as well in imaging natural gas hydrate recovered from marine and subpermafrost settings (Kuhs et al., 2004). Their SEM investigations also revealed the remarkable development of 'mesoporous' gas hydrate (i.e. pervasive submicrometre-sized pore development) formed by reaction of gas with ice at temperatures near the ice point. The present authors have also reported on SEM investigations of gas hydrate samples from both laboratory and natural origin, including pure methane hydrate (±sediments) at various extents of reaction and recrystallization (Stern et al., 2004a), dissociation and dissolution textures (Stern et al., 2002, 2003, 2004a), compaction and deformation textures (Durham et al., 2003a), pure, porous CO_2 and propane hydrate (Circone et al., 2003; Stern et al., 2004a), and natural gas hydrate from the Gulf of Mexico (Stern and Kirby, 2004; Stern et al., 2004a). The present authors have also imaged numerous gas-hydrate-bearing samples with known fractions of ice, as well as samples used in surface sublimation or partial decomposition tests (Stern et al., 2004a) to specifically address the question of distinguishing gas hydrate from ice.

For the study of gas hydrate samples recovered from natural or otherwise remote settings, these challenges are amplified by such additional unknowns as the complex in situ environmental conditions controlling the original growth textures, and any effects of subsequent recrystallization, annealing, secondary growth, dissociation, dissolution, or chemical exchange processes. The extent of sample damage or alteration incurred during retrieval of the gas hydrate presents additional unknowns. Lacking a wider sampling archive and long-term experience in assessing these issues, it is presumed that most interpretations of SEM images of natural gas hydrate samples are still somewhat speculative. Nonetheless, useful information about grain structure, pore characteristics, phase composition, and phase distribution may still be gleaned from even exploratory investigations, particularly if natural gas hydrate can be compared to other materials with precisely known composition and histories.

Here, a 'first look' at some natural gas-hydrate-bearing samples recovered from JAPEX/JNOC/GSC et al. Mallik 5L-38 is presented (Dallimore and Collett, 2005; *see also* Techmer et al., 2005), and the observed features are compared to those documented previously in lab-synthesized gas hydrate samples of known composition, grain structure, pressure-temperature (P-T) processing histories, and compaction or deformation history. These results are largely qualitative, as only limited compositional information on the natural gas hydrate can be collected at this time. Instead, preliminary interpretations drawn from comparisons with the SEM image archive are presented. Lastly, the geometrical arrangement of phases observed in several Mallik samples from sand intervals are compared to those of mixed-phase aggregates formed in the lab, and implications of such comparisons are discussed. Benefits of pursuing comparative studies of natural and synthetic samples are the relative low cost, ease, and reproducibility of creating gas-hydrate-bearing samples in the lab with well characterized phases in known concentrations and geometrical arrangements, and the ability to isolate or introduce additional complexities in a controlled manner.

EXPERIMENTAL METHODS

Samples from Mallik 5L-38 arrived in a liquid nitrogen 'dry' vapor shipper, in which each sample was individually sealed within a plastic container. A small amount of free liquid nitrogen was present in the base of the shipper upon arrival, indicating that samples remained stable during transit.

SEM preparation and imaging procedures

For SEM imaging, small sections of samples (~0.5 cm x 0.5 cm x 0.75 cm) were cleaved under liquid nitrogen from the bulk samples, transferred to a sample stage within an evacuated and prechilled (below 100 K) cryo-preparation and coating station (Gatan Alto Model 2100), which was in turn attached to a LEO 982 field emission SEM. While still in the preparation chamber, the section was again cleaved by cold blade to produce fresh fracture surfaces for imaging that were not contaminated by surface-water condensation. A few samples were coated with AuPd for 60 s using a non-heat-emitting sputter head, but most were imaged uncoated to avoid increased time under vacuum exposure. Samples, still under vacuum conditions, were then inserted directly through the back of the preparation chamber and onto an auxiliary cryo-imaging stage in the SEM column. Sample temperature was continuously

monitored by thermocouples, one embedded just below the surface of the preparation-chamber sample stage, and one placed identically within the sample stage of the SEM chamber. Imaging was conducted at temperatures below 102 K and vacuum below 10^{-6} kPa (10^{-5} mbar), and conditions were monitored by gauge displays on the cryo-stage control unit. Low voltage (usually ≤2 kV) was used during imaging to minimize sample alteration or beam damage of the sample surface, increasing voltage to 5 kV or 10 kV only for EDX (energy dispersive X-ray spectroscopy) procedures (discussed below). Several imaged areas were re-examined near the end of every SEM session to monitor any changes in surface topology over time, such as that produced by beam damage, vacuum damage, or sublimation effects, in order to avoid misinterpretating measurement-induced morphologies as original growth features. Further details of preparation and imaging procedures are given in Stern et al. (2004a).

Phase identification, in certain cases, was problematic. Port requirements necessitated the removal of the back-scattered electron detector when the cryosystem was in use. Gas hydrate could often be distinguished from ice using the instrument's EDX capabilities, but resolution was limited by the long focal distance (~15 mm) needed for this technique combined with the relatively low accelerating voltage needed to minimize sample damage. Carbon peaks were small, but identifiable by EDX in dense grains of methane hydrate (Fig. 1), but often impossible to resolve in uneven, porous, or partially dissociated samples.

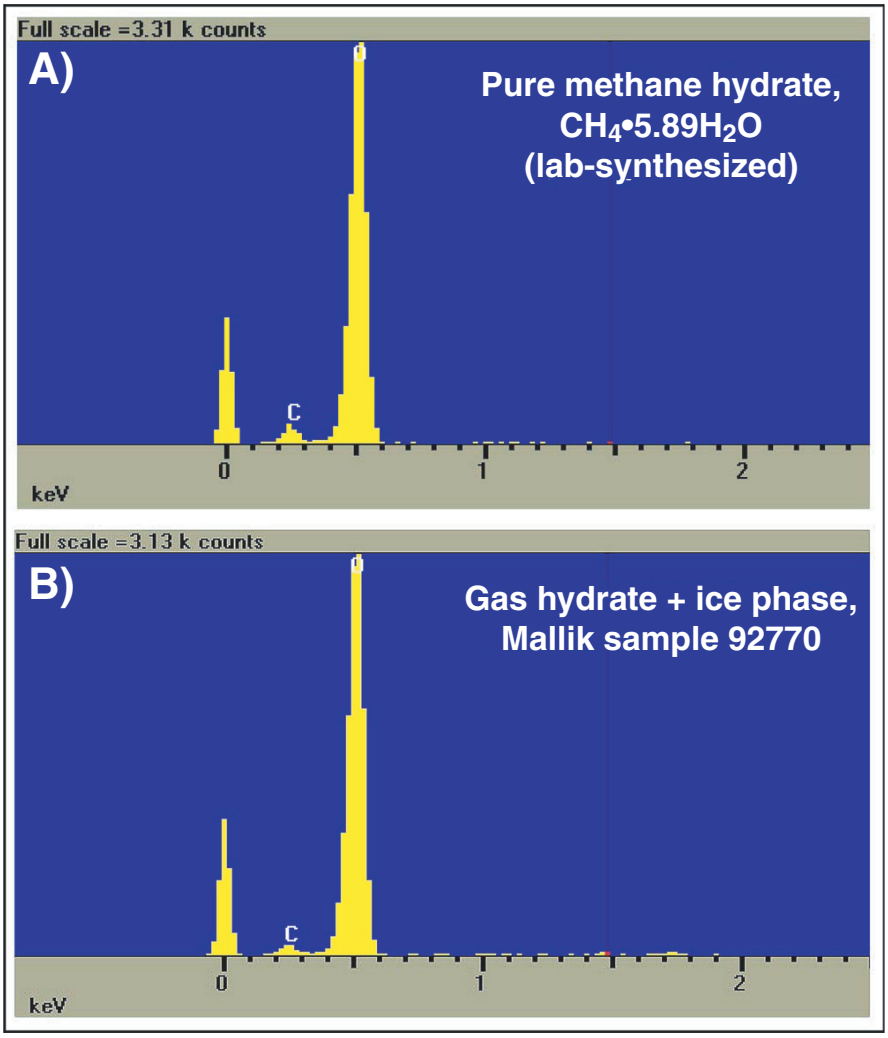

Figure 1. *Energy dispersive X-ray spectroscopy scans of pure methane hydrate with* ***A)*** *known stoichiometry compared to* ***B)*** *a 'smooth' section (*see *Fig. 2) of gas hydrate from Mallik sample 92770. The carbon peak (indicated by 'C' on the scans) is small even in pure gas hydrate samples with close to ideal methane content, so the presence of the peak in the Mallik scan is encouraging in that the sample contains a significant fraction of undissociated gas hydrate. Highly dissociated samples or those with rough surfaces tend to yield patterns with no measurable carbon peak, like ice. Both samples shown here were measured at 10 kV, at a 15 mm focal distance.*

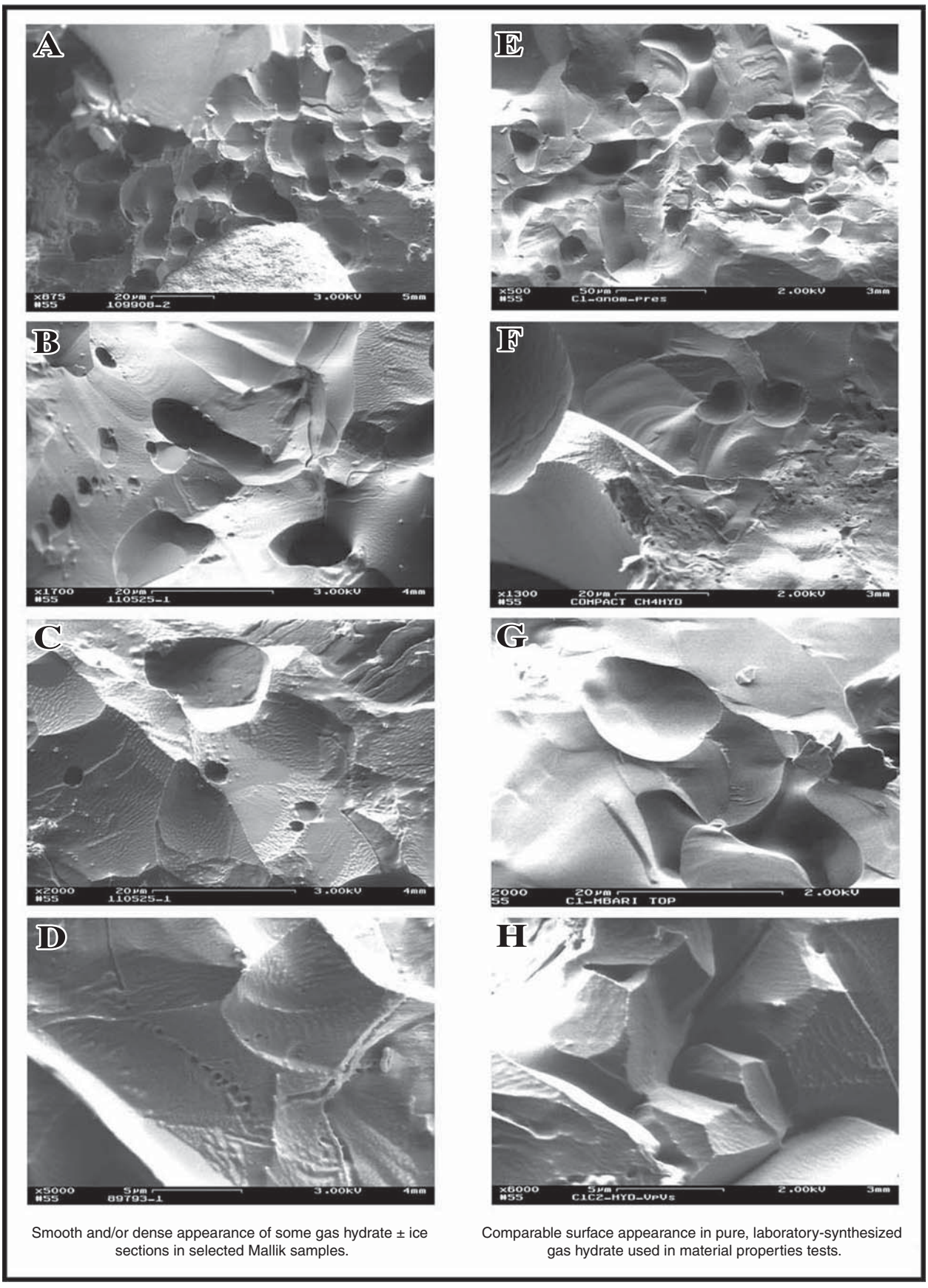
A
B
C
D
E
F
G
H
Smooth and/or dense appearance of some gas hydrate ± ice sections in selected Mallik samples.
Comparable surface appearance in pure, laboratory-synthesized gas hydrate used in material properties tests.

Figure 2.

Laboratory gas hydrate: synthesis

Laboratory-synthesized gas hydrate samples used for visual comparisons in this study were synthesized by warming fine-grained (~200 μm) ice in the presence of gas-hydrate-forming gas or liquid (*see* Stern et al. (1996, 2000) for further description). Synthesis of gas hydrate in sediments involved the premixing or layering of sediment particles with the granular ice in the reaction vessel prior to admission of the gas-hydrate-forming gas. Despite substantial melting within many of the ice grains, minimal migration of either water or sediment accompanies reaction, allowing fabrication of 'custom' samples with a variety of predetermined textures or layering sequences (shown in Fig. 4 *in* Stern et al. (2000)). Alternatively, sediment can be mixed or layered with pure gas hydrate grains inside of a supporting soft-metal jacket prior to hydrostatic compaction. Synthesis methods for the laboratory-tested samples shown in Figures 2 and 3 are detailed in the references given in the respective figure captions.

Laboratory gas hydrate samples: compaction and mechanical testing

Compaction and strength testing of the laboratory samples shown in Figures 4 and 5b was conducted in a triaxial gas apparatus specially designed for low-temperature use (Durham et al., 2003a). Standard rock mechanics experimental methods were used, including encapsulating the sample materials and testing at elevated confining pressures to suppress macroscopic fracture (*see* Durham et al. (2003a, b) for further description). Samples were tested under either creep (constant deviatoric stress) or constant-strain-rate conditions, at confining pressures of 50 MPa and 100 MPa, pore pressures of 1.6 MPa to 15 MPa to maintain samples within their equilibrium stability field, and temperatures bracketing the ice point ($260\ K \leq T \leq 287\ K$). Following testing, samples were slowly cooled under pressure to below 150 K, then further cooled, depressurized, removed, and stored in liquid nitrogen for subsequent imaging by SEM.

RESULTS AND DISCUSSION

Surface morphology and material density of the gas hydrate phase

Scanning electron microscopy imaging of a selection of Mallik samples reveals a wide variety of grain morphologies and textures. A representative collection of images is assembled in the Appendix to this paper. X-ray diffraction measurements on gas-hydrate-bearing samples from several intervals within Mallik 5L-38 show that volumetric ratios of gas hydrate-to-ice are in the range of 40–48% (Uchida et al., 2005). As discussed above and shown in Figure 1, however, clear distinction between ice and gas hydrate phases is often problematic. The Appendix images are therefore presented primarily to offer a general sense of sample appearance and textural variation at both high- and low-magnification perspectives. Sediment particles within the samples can be clearly identified by their shape and stance in raised relief, whereas the pore-filling material is a mixture of sI gas hydrate and ice.

Without detailed understanding of the complete history of the field samples, however, distinguishing between the textures or structures produced in situ and those produced during core recovery remains challenging. Surface morphology and texture of the gas hydrate phase is particularly difficult to interpret with confidence. Scanning electron microscopy imaging reveals that the gas hydrate (± ice) phase exhibits two general physical states: as a dense material surrounding large macropores (Fig. 2A–D), and as a sponge-like, highly 'mesoporous' material (Fig. 3A–D). Both of these habits appear in most samples, often closely juxtaposed or interconnected.

Understanding the mechanisms or processes that promote development of mesoporosity in gas hydrate, and establishing whether it is original growth or merely an artifact of recovery procedures, has important consequences. Such texture can have measurable effects, for instance, on properties such as thermal conductivity and acoustic velocity. Alternatively, if the texture is largely due to partial dissociation, then the additional 'contaminant' ice phase can further complicate interpretations of measurements since ice and gas hydrate properties can be quite different.

Growth of such an apparently nonequilibrium texture is enigmatic, as the porous microstructure develops at the free-energy cost of additional gas hydrate surface energy. Mesoporous growth was first reported by Kuhs et al. (2000) in a variety of gas hydrate samples grown from ice in the presence of excess gas. Development of the subporous microstructure was investigated further by Salamatin and Kuhs (2002), Staykova et al. (2003), Klapproth et al. (2003), and Genov et al. (2004), all of which provided excellent treatment and quantitative assessment of this growth process and its role and relevance to growth kinetic models at temperatures primarily below the ice point, or to its possible influence on macroscopic properties (Kuhs et al., 2004). In recent work, the present authors have also imaged and reported on initial growth of gas

Figure 2. *Side-by-side comparison showing some close similarities in the morphologies of selected sections of the gas hydrate (± ice) phase in Mallik samples* ***(A–D*** *with sample numbers shown with scale bars beneath each photograph) compared to laboratory-synthesized samples with known composition and P-T processing histories* ***(E–H); E)*** *pure methane hydrate after 'anomalous' or 'self-preservation' tests (Stern et al., 2003);* ***F)*** *pure, partially compacted methane hydrate after thermal conductivity tests (Waite et al., 2002a, b);* ***G)*** *pure methane hydrate recovered after ocean-floor dissolution experiments (Stern et al., 2002; Rehder et al., 2004); and* ***H)*** *pure, sII methane-ethane hydrate after ultrasonic wave-speed measurement (Helgerud et al., 2003). The material density, pore size, and pore connectivity displayed by these gas hydrate samples is in marked contrast to the pervasive mesoporosity exhibited in Figure 3.*

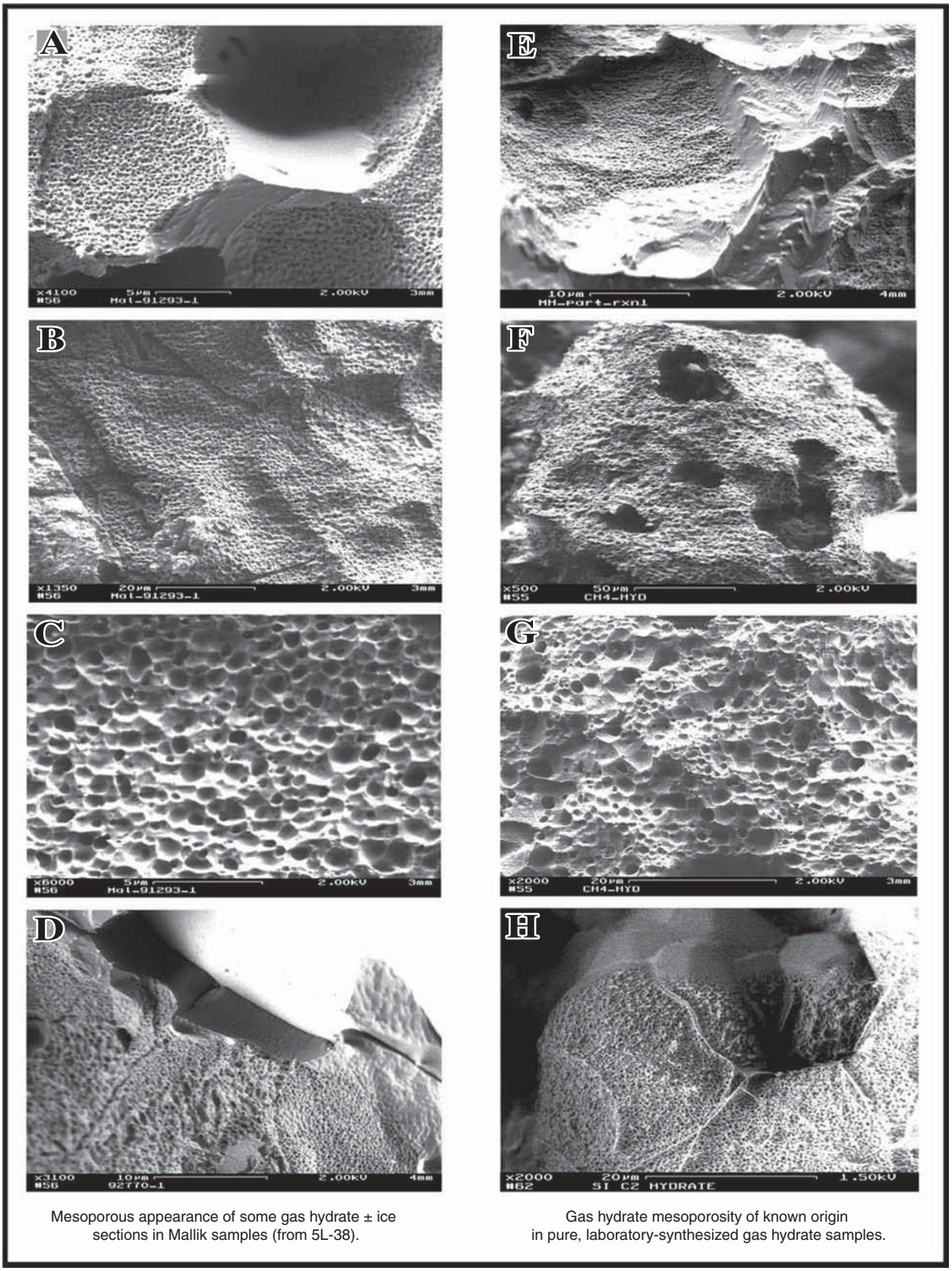

Mesoporous appearance of some gas hydrate ± ice sections in Mallik samples (from 5L-38).

Gas hydrate mesoporosity of known origin in pure, laboratory-synthesized gas hydrate samples.

Figure 3.

hydrate from ice as a mesoporous growth front advancing into the dense ice reactant (Stern et al., 2004a). An example is shown in Figure 3E. Extremely similar textures, however, can be produced by dissociation of originally dense grains of gas hydrate to ice, as illustrated in Figures 3F and 3G. Moreover, prolonged exposure of gas hydrate to high vacuum conditions in the SEM column can also produce surface deterioration or breakdown with near-identical appearance (Fig. 3H). Figure 3 illustrates that not only are these lab-made examples virtually identical, but they also closely resemble certain textures observed in the Mallik samples.

At the present time there is no definitive means of establishing the origin of mesoporosity in the Mallik samples, due to the many environmental unknowns involved in their formation and recovery history. However, in previous investigations of growth and recrystallization processes in gas hydrate samples (Stern et al., 2004a), mesoporosity was captured only as a transient morphology that persisted primarily during early- to mid-stages of synthesis from ice+gas mixtures. Original-growth mesoporosity was never observed in any samples that were synthesized or subsequently held above the ice point for extended time, or in any samples in contact with an aqueous liquid phase. Instead, the initially porous gas hydrate was always found to anneal to dense material, as shown in Figures 2E–H. Although it could be argued that the dense gas hydrate material in Mallik samples shown in Figures 2A–D is, instead, annealed from initially grown mesoporous gas hydrate, or the result of dissociation of mesoporous gas hydrate followed by melting and refreezing, the positive identification of carbon peaks in the dense material, combined with the observations of known formation textures as outlined above, suggests otherwise. The dense material also exhibits obvious degassing when removed from the SEM and warmed. The mesoporosity exhibited by the Mallik samples is thus likely, but not conclusively, an artifact of partial dissociation to an ice product. The relatively long-term stability of mesoporous sections of Mallik samples under the SEM beam compared to that observed for laboratory samples also supports this hypothesis. Whether mesoporosity can remain stable on the geological time scale, particularly in permafrost-type environments, remains an intriguing question for further investigation.

'Emulation' of natural gas hydrate samples in the lab – what can we learn?

Until recently, evaluating or modelling the effects of hydrocarbon clathrate hydrate on sediment properties was difficult because many of the fundamental physical properties had not been directly measured on pure end-member gas hydrate samples, and particularly, methane hydrate. Ordinary water ice and gas hydrate share similarities in the nature of the hydrogen bonds forming the framework of their open structures, and many of the material properties of ice have thus commonly been used in lieu of direct measurements on hydrocarbon hydrate. This assumption seems reasonable at first glance; gas hydrate is approximately 85 mol % water even with all cages occupied (Sloan, 1998), and shares similarities in the H_2O molecular bonding of the lattices compared to ice.

In the case of mechanical properties, however, this assumption has recently been proven invalid. End-member gas hydrate —at least those tested to date — are in fact exceptionally strong relative to ice. Triaxial compression tests show that pure sI methane hydrate, sI CO_2 hydrate, and sII methane-ethane hydrate all have ductile flow strengths that are 20 times to upward of 100 times stronger than ice under the same conditions, and in fact even have different rheologies than each other (Durham et al., 2003a, b; Stern et al., 2004b). Figure 5 shows some physical expressions of the very high plastic flow strength of methane hydrate relative to water ice. At 260 K and strain rate 3.5 x 10^{-6} s^{-1}, for example, the steady-state stress supported by polycrystalline water ice is only about 1.5 MPa, compared to about 48 MPa for pure methane hydrate. These findings suggest that the effects of gas hydrate in increasing the strength or cohesion of sediments is likely considerably larger than the effects of ice in arctic permafrost. By corollary, such strengthening effects are then lost during gas hydrate decomposition, and it is important to note that this weakening effect of dissociation is in addition to the pore-pressure effect of gas release.

Scanning electron microscopy imaging of gas hydrate in Mallik drill core now provides additional information on gas hydrate–sediment grain distribution and contact, and allows fabrication and testing of aggregate materials in the laboratory with comparable arrangements and distribution of phases. Key advantages in synthesizing such samples in the laboratory include the ease of fabrication with no secondary ice phase, and the ability to work with sediment 'standards' with known properties, both of which greatly simplify interpretations of subsequent measurements and results.

Figure 4 shows a lab-synthesized sample of pure methane hydrate mixed with about 50 volume per cent quartz sand, after full compaction and rheological testing, illustrating the similarity in general appearance with selected samples from the Mallik wells. Test measurements made on this sample indicate that adding a nearly homogeneous distribution of 50 volume per cent quartz to methane hydrate serves to increase

Figure 3. *Side-by-side comparisons of mesoporous surface texture evident in certain sections of the gas hydrate ± ice fraction in Mallik samples (**A–D**) with laboratory samples of known composition and histories (**E–H**). The density of the gas hydrate (and/or ice) is in sharp contrast to that shown in Figure 2, here displaying a 'spongy' appearance resulting from extensive development of submicrometre-sized pores. Mesoporosity in gas hydrate can be produced during initial growth as well as from partial dissociation or surface damage, in all cases appearing virtually identical. Examples with known source or known mechanism for the mesoporosity are shown at right: as an original growth texture in **E**, as a result of low-temperature partial decomposition to ice in **F** and **G**, and as a result of exposure to high vacuum conditions within the SEM column in **H**. Samples shown in **F**, **G**, and **H** were fully dense prior to their partial dissociation or sublimation.*

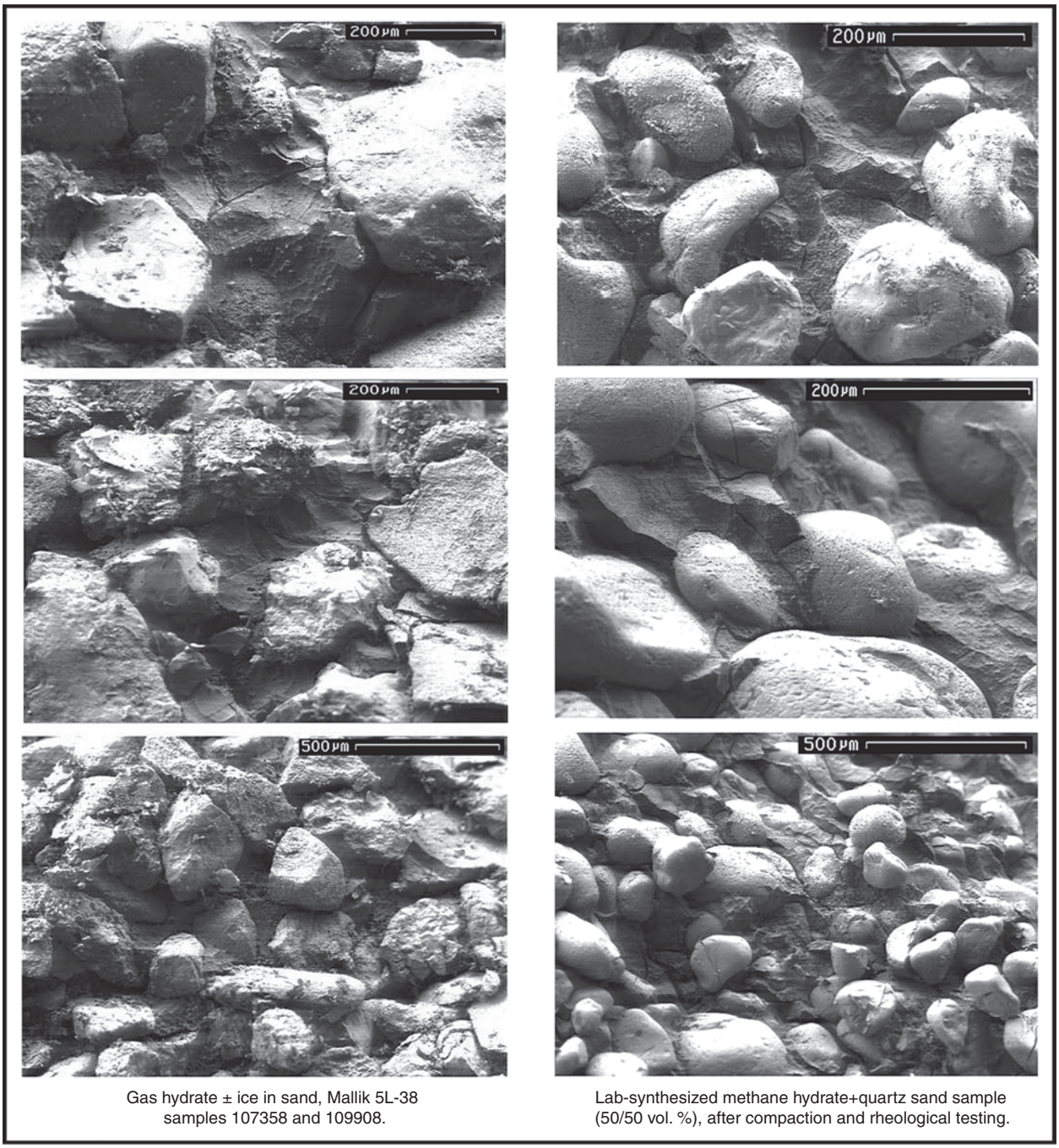

Figure 4. *Side-by-side images of the gas hydrate fraction in sand intervals from the Mallik site, compared to methane hydrate + quartz sand aggregate formed in the laboratory and used in subsequent compaction and strength measurement experiments. The rounded grains in all images are sediment, and in the right-hand column, are a pure quartz sand standard with average grain size of 100 µm. In both the Mallik and lab samples, the gas hydrate phase forms a very strong load-bearing cement that occurs between sediment grains and often encompasses them. Rheological testing on the lab sample at right shows that the addition of 50 volume per cent quartz dispersed nearly homogeneously through the gas hydrate increases the strength by only about a factor of two compared to pure methane hydrate at temperatures relevant to the Mallik site. In comparison to ice, however, the strength contrast is dramatic. See Figure 5 and text for further discussion.*

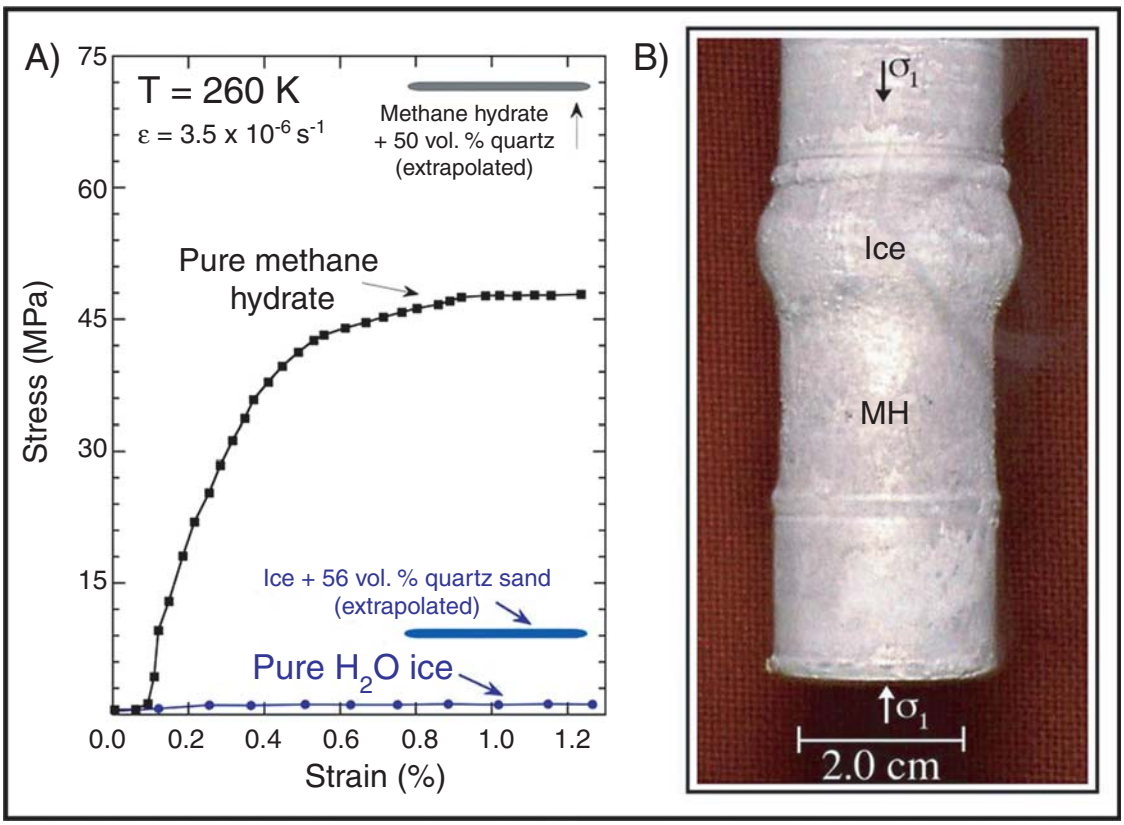

Figure 5. *Manifestations of the exceptional strength contrast between pure methane hydrate and pure water ice:* ***A)*** *Stress-strain curves for samples of pure methane hydrate versus ice, each tested at –13°C with confining pressure 100 MPa, at strain rate of 3.5 x 10^{-6} s^{-1}. Under these conditions, methane hydrate is roughly 30 times stronger than ice, and this strength contrast increases with decreasing temperature. The extrapolated steady-state stress for samples of methane hydrate + 50 vol. % quartz sand (sample shown in Fig. 4), and for ice + 56 vol. % quartz sand (using same quartz sand standard) are also shown for comparison. (The mixed-phase aggregates were tested at conditions above and below 260 K, hence the extrapolation. See text for further discussion.)* ***B)*** *Indium-jacketed composite sample of ice (top) and methane hydrate (MH) after compression testing in the laboratory. The sample was a near-perfect cylinder prior to testing. The post-test appearance of the sample shows that virtually all the sample strain is accommodated in the (weaker) ice phase. Figures 5A and 5B modified from figures discussed in greater detail in Durham et al. (1992, 2003a, b) and Stern et al. (2004b).*

the strength by nearly a factor of two at test temperatures of 270–280 K (Stern et al., 2004b). This effect is roughly comparable, although somewhat less pronounced, than the effect of adding the same quartz sand standard to pure ice (Fig. 5A).

These results are merely the first step in emulating Mallik material, and are not intended for quantitative modelling or prediction purposes. Instead, they are intended to provide perspective on the strength contrasts of pure gas hydrate and ice, and the relative effects of adding gas hydrate or ice to the same sediment matrix, in proportions roughly comparable to those displayed in certain samples from the Mallik 5L-38 well. Uchida et al. (2005) provided additional strength measurements made on actual recovered material, but comparisons remain difficult due the unknown effects of secondary mineralogy or of contaminant ice. Previous measurements (Stern et al., 1996), for example, showed that methane hydrate + ice samples that contained only 25 volume per cent ice behaved virtually 'ice like' in respect to the steady-state stresses they supported, indicating a very strong influence of the weaker ice phase within the mixed-phase samples. Considerable additional testing is also needed to fully explore the many effects and complexities that sediments, in different sizes, concentrations, and distributions, may introduce. Clay minerals that occur in Mallik intervals (*see* Medioli et al., 2005) and organic phases have not yet been included within synthetic samples from this study, yet may affect aggregate strength or properties, or even gas hydrate distribution. Further testing is also needed to determine whether the addition of particulates to gas hydrate produces 'toughening' or other work- hardening effects similar to those exhibited by ice-sediment mixtures (Durham et al. 1992). The porosity in recovered Mallik 5L-38 samples is typically lower than 40%

(Uchida et al., 2005), so the gas hydrate volume in our synthetic samples is more than the normal pore volume after compaction. Additionally, the exact nature of the gas hydrate–sediment grain contacts is not well established, in part due to the difficulty in differentiating original from secondary ice in recovered, natural samples. Obviously, there remain many outstanding issues to address. These first results do, however, help refine the understanding of how gas hydrate may affect sediment strength in relation to the effects of ice. Moreover, the textural similarities exhibited by these two classes of samples give reason to believe that processes that govern the structural development of at least some natural gas hydrate in sediments can be emulated.

SUMMARY: IMPLICATIONS FOR FURTHER INVESTIGATIONS

While significant progress has been achieved in these first few years of applying cryo-SEM imaging techniques to gas hydrate studies, the technique is still most confidently applied to samples with 1) known phase composition, stoichiometry, and grain morphology or fabric; 2) known origin, distribution, and amount of any ice occurring as either an original or secondary 'contaminant' phase; and 3) known pressure-temperature history and possible fluid-phase interaction. Such samples, at this point, are still those that are produced in the closely controlled environment of the laboratory, and are also the most suitable for end-member physical- and material-property testing. Nonetheless, cryogenic SEM provides a powerful means for investigating how closely synthetic samples emulate the complexity inherent to natural gas-hydrate-bearing material. This study shows that not only do Mallik samples exhibit a variety of textures and grain morphologies associated with the gas hydrate phase, but that at least in some instances, it is possible to emulate their complexity, or at least identify certain textural aspects that require further investigation.

Despite the many unknowns associated with any gas hydrate recovered from remote settings, samples recovered from (or below) arctic permafrost regions should not undergo significant migration of phases during recovery, at least in comparison to samples recovered with significant pore water within them, or samples subjected to multiple warming, cooling, and/or repressurization cycles during recovery attempts. Hence, SEM imaging of Mallik-type gas hydrate may be not only beneficial in the elucidation of the general appearance of the samples, but also in revelation at the microscale of specific geometrical distributions and arrangements of phases, which in turn, can be used as 'templates' for synthesis of gas hydrate–sediment samples in the laboratory. Here, the gas hydrate + sand interval has been used as an example, and preliminary experiments aimed at understanding the mechanical behavior of such aggregate materials have been described. While these experiments represent only a first step in understanding the mechanical effects and influences of gas hydrate, future tests and measurements on gas hydrate–sediment aggregates with known phase articulation, based on geometrical arrangements displayed by natural samples, should further improve the understanding of the possible effects of gas hydrate on elastic and inelastic properties of formations in which they may occur. Further tests and imaging of laboratory-synthesized samples should also help relate measurements to those made on either recovered or in situ gas-hydrate-bearing material, and in turn, to appropriate rock-physics models.

ACKNOWLEDGMENTS

The authors acknowledge the international partnership that undertook the Mallik 2002 Gas Hydrate Production Research Well Program: the Geological Survey of Canada (GSC), Japan National Oil Corporation (JNOC), GeoForschungsZentrum Potsdam (GFZ), United States Geological Survey (USGS), United States Department of Energy (USDOE), India Ministry of Petroleum and Natural Gas (MOPNG), and BP-ChevronTexaco-Burlington joint venture parties. The program received financial support from the International Continental Scientific Drilling Program (ICDP). Work presented here was supported by the USGS Gas Hydrate Project and NASA's Planetary Geology and Geophysics Program. Work by W.B. Durham was performed under the auspices of the USDOE by the Lawrence Livermore National Laboratory under contract W-7405-ENG-48. The authors thank R. Oscarson, J. Pinkston, and S. Circone of the USGS for technical assistance, and W. Waite (USGS), T. Lorenson (USGS), K. Techmer (GZG Gottingen), and one anonymous referee for helpful reviews of the manuscript.

REFERENCES

Circone, S., Stern, L., Kirby, S., Durham, W., Chakoumakos, B., Rawn, C., Rondinone, A., and Ishii, Y.
2003: CO_2 hydrate: synthesis, composition, dissociation behavior, and a comparison to structure I CH_4 hydrate; Journal of Physical Chemistry B, v. 107, p. 5529–5539.

Dallimore, S.R. and Collett, T.S.
2005: Summary and implications of the Mallik 2002 Gas Hydrate Production Research Well Program; *in* Scientific Results from the Mallik 2002 Gas Hydrate Production Research Well Program, Mackenzie Delta, Northwest Territories, Canada, (ed.) S.R. Dallimore and T.S. Collett; Geological Survey of Canada, Bulletin 585.

Durham, W., Kirby, S., and Stern, L.
1992: Effects of dispersed particulates on the rheology of water ice at planetary conditions; Journal of Geophysical Research, v. 97, no. E12, p. 20 883–20 897.

Durham, W., Kirby, S., Stern, L., and Zhang, W.
2003a: The strength and rheology of methane clathrate hydrate; Journal of Geophysical Research, v. 108, no. B4, p. 2182–2193.

Durham, W., Stern, L., and Kirby, S.
2003b: Ductile flow of methane hydrate; Canadian Journal of Physics, v. 81, no. 1-2, p. 373–380.

Genov, G., Kuhs, W., Staykova, D., Goreshnik, E., and Salamatin, A.
2004: Experimental studies of the formation of porous gas hydrates; American Mineralogist, v. 89, no. 8-9, p. 1228–1239.

Helgerud, M., Waite, W., Kirby, S., and Nur, A.
2003: Measured temperature and pressure dependence of Vp and Vs in compacted, polycrystalline sI methane and sII methane-ethane hydrate; Canadian Journal of Physics, v. 81, no. 1-2, p. 47–53.

Klapproth, A., Goreshnik, E., Staykova, D., Klein, H., and Kuhs, W.
2003: Structural studies of gas hydrates; Canadian Journal of Physics, v. 81, no. 1-2, p. 503–518.

Kuhs, W., Genov, G., Goreshnik, E., Zeller, A., Techmer, K., and Borhmann, G.
2004: The impact of porous microstructures of gas hydrates on their macroscopic properties; *in* Proceedings of the 14th International Offshore and Polar Engineering Conference, Toulon, France, May, 2004, p. 31–35.

Kuhs, W., Klapproth, A., Gotthardt, F., Techmer, K., and Heinrichs, T.
2000: The formation of meso- and macroporous hydrates; Geophysical Research Letters, v. 27, p. 2929–2932.

Medioli, B.E., Wilson, N., Dallimore, S.R., Paré, D., Brennan-Alpert, P., and Oda, H.
2005: Sedimentology of the cored interval, JAPEX/JNOC/GSC et al. Mallik 5L-38 gas hydrate production research well; *in* Scientific Results from the Mallik 2002 Gas Hydrate Production Research Well Program, Mackenzie Delta, Northwest Territories, Canada, (ed.) S.R. Dallimore and T.S. Collett; Geological Survey of Canada, Bulletin 585.

Rehder, G., Kirby, S., Durham, W., Stern, L., Peltzer, E., Pinkston, J., and Brewer, P.
2004: Dissolution rates of pure methane hydrate and carbon dioxide hydrate in undersaturated seawater at 1000 m depth; Geochimica et Cosmochemica Acta, v. 68, p. 285–292.

Salamatin, A. and Kuhs, W.
2002: Formation of porous gas hydrates; *in* Proceedings of the 4th International Conference on Gas Hydrates, Yokohama, Japan, 2002, p. 766–770.

Sloan, E.D., Jr.
1998: Clathrate Hydrates of Natural Gases (revised edition); Marcel Dekker, Inc., New York, Basel, 705 p.

Staykova, D., Kuhs, W., Salamatin, A., and Hansen, T.
2003: Formation of porous gas hydrate from ice powders: diffraction experiments and multi-stage model; Journal of Physical Chemistry B, v. 107, p. 10 299–10 311.

Stern, L. and Kirby, S.
2004: Grain and pore structure imaging of gas hydrate from core MD02-2569 (West Mississippi Site, Gulf of Mexico): a first look by SEM; *in* Initial Report of the IMAGES VIII/PAGE 127 Gas Hydrate and Paleoclimate Cruise on the RV Marion Dufresne in the Gulf of Mexico, 2–18 July 2002, (ed.) W.J. Winters, T.D. Lorenson, and C.K. Paull; United States Geological Survey, Open File Report 2004-1358.

Stern, L., Circone, S., Kirby, S., and Durham, W.
2003: Temperature, pressure, and compositional effects on anomalous or "self" preservation of gas hydrates; Canadian Journal of Physics, v. 81, no. 1-2, p. 271–283.
2004a: Application of Scanning Electron Microscopy (SEM) to investigate growth and annealing of gas clathrate hydrates formed from melting ice; American Mineralogist, v. 89, no. 8-9, p. 1162–1175.

Stern, L., Durham, W., Kirby, S., Circone, S., and Helgerud, M.
2004b: Experimental observations pertinent to the mechanical and thermal stability of sI methane hydrate/sand aggregates; *in* Extended Abstract, American Association of Petroleum Geologists Annual Meeting 2004, Dallas, Texas (CD-ROM).

Stern, L., Kirby, S., Durham, W., Circone, S., and Waite, W.
2000: Synthesis of pure methane hydrate suitable for measurement of physical properties and decomposition behavior; Chapter 25 *in* Natural Gas Hydrate in Oceanic and Permafrost Environments, (ed.) M.D. Max; Kluwer, Dordrecht, p. 323–349.

Stern, L., Peltzer, E., Durham, W., Kirby, S., Brewer, P., Circone, S., and Rehder, G.
2002: Dissolution of hydrocarbon gas hydrates in seawater at 1030 meters; effects of porosity, structure, and compositional variation as determined by high-definition video and SEM imaging; EOS, Transactions of the American Geophysical Union, v. 83, abstract OS21B-0216, p. F777.

Stern, L.A., Kirby, S.H., and Durham, W.B.
1996: Peculiarities of methane clathrate hydrate formation and solid-state deformation, including possible superheating of water ice; Science, v. 273, p. 1843–1848.

Techmer, K.S., Heinrichs, T., and Kuhs, W.F.
2005: Cryo-electron microscopic studies of structures and composition of Mallik gas-hydrate-bearing samples; *in* Scientific Results from the Mallik 2002 Gas Hydrate Production Research Well Program, Mackenzie Delta, Northwest Territories, Canada, (ed.) S.R. Dallimore and T.S. Collett; Geological Survey of Canada, Bulletin 585.

Uchida, T., Uchida, T., Kato, A., Sasaki, H., Kono, F., and Takeya, S.
2005: Physical properties of natural gas hydrate and associated gas-hydrate-bearing sediments in the JAPEX/JNOC/GSC et al. Mallik 5L-38 gas hydrate production research well; *in* Scientific Results from the Mallik 2002 Gas Hydrate Production Research Well Program, Mackenzie Delta, Northwest Territories, Canada, (ed.) S.R. Dallimore and T.S. Collett; Geological Survey of Canada, Bulletin 585.

Waite, W., de Martin, B., Pinkston, J., Kirby, S., and Ruppel, C.
2002a: Thermal conductivity measurements in porous mixtures of methane hydrate and quartz sand; Geophysical Research Letters, v. 29, p. 2229.

Waite, W., Pinkston, J., and Kirby, S.
2002b: Preliminary laboratory thermal conductivity measurements in pure methane hydrate and methane hydrate-sediment mixtures: a progress report; *in* Proceedings of the 4th International Conference on Gas Hydrates, Yokohama, Japan, 2002, p. 728–733.

APPENDIX

Scanning electron microscopy image gallery of some JAPEX/JNOC/GSC et al. Mallik 5L-38 gas-hydrate-bearing samples.

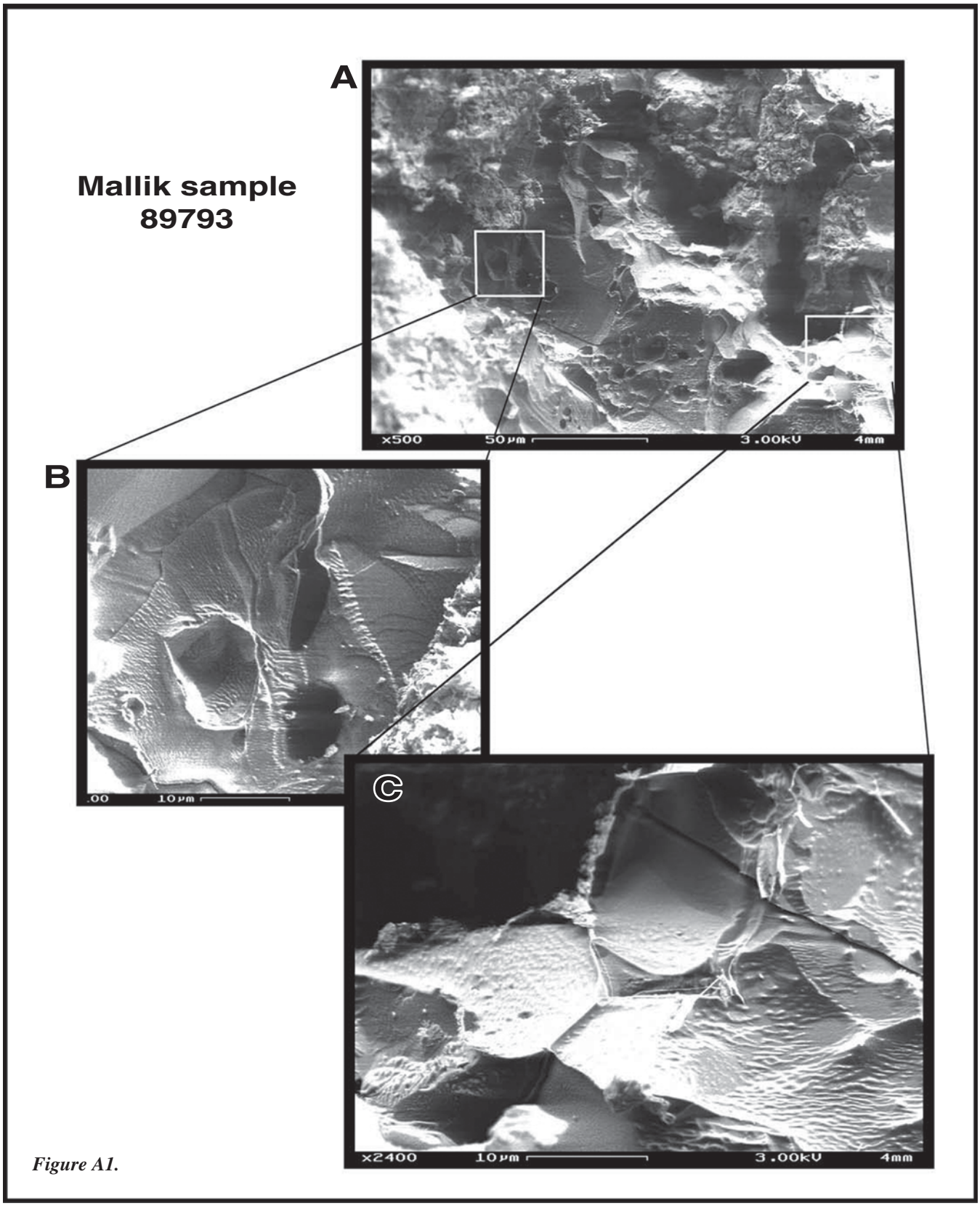

Figure A1.

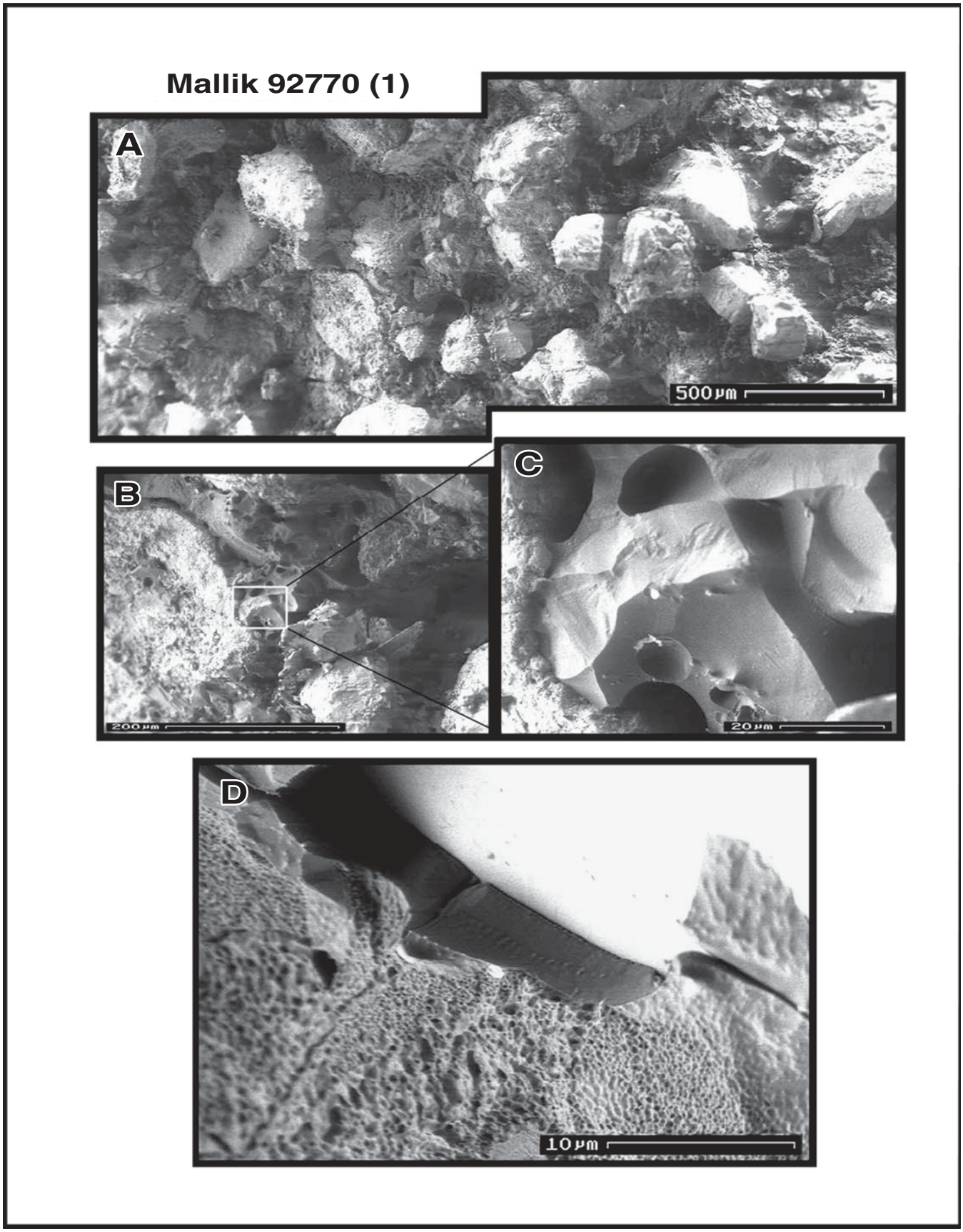

Figure A2.

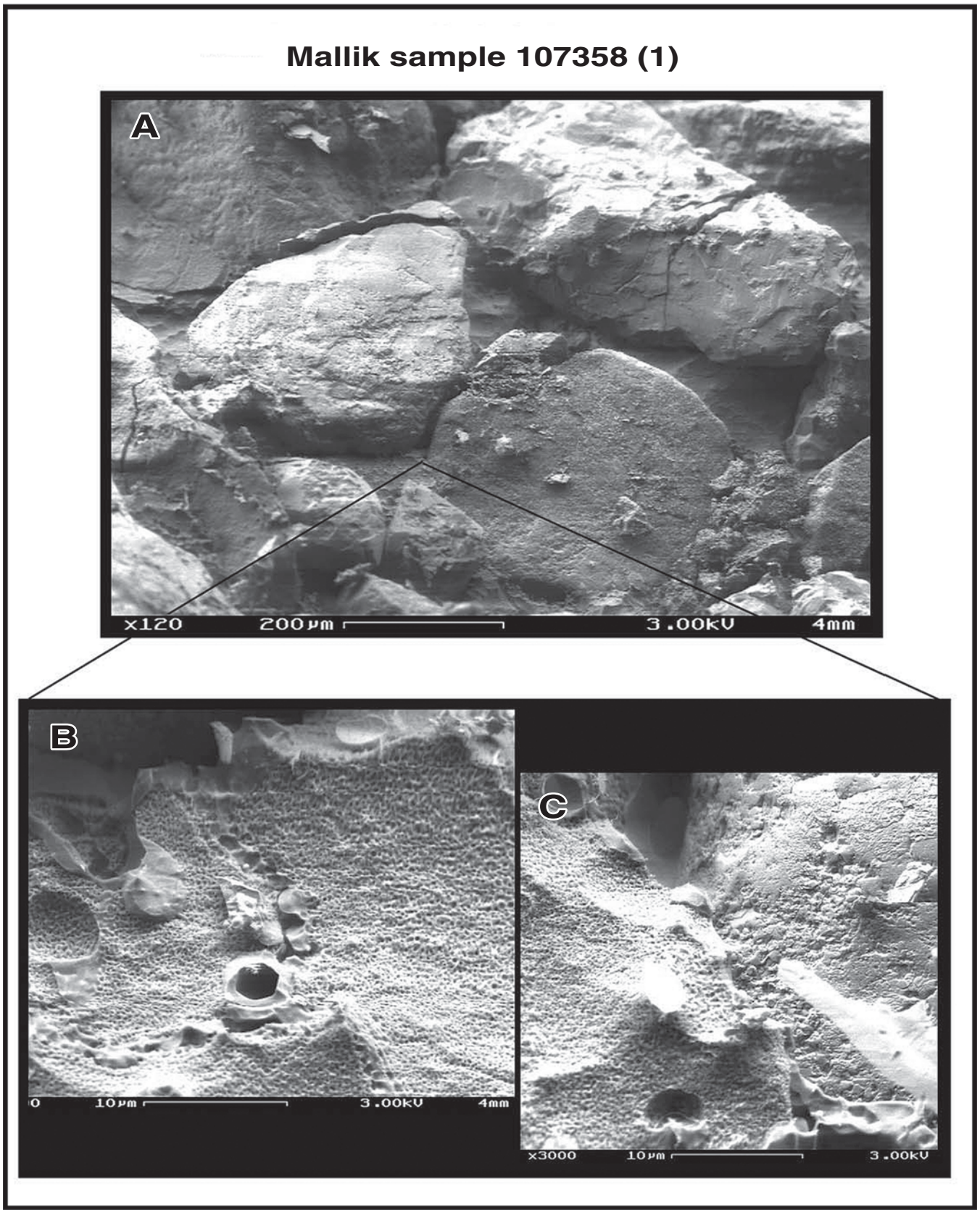
Mallik sample 107358 (1)
A
x120 200µm 3.00kV 4mm
B
10µm 3.00kV 4mm
C
x3000 10µm 3.00kV

Figure A3.

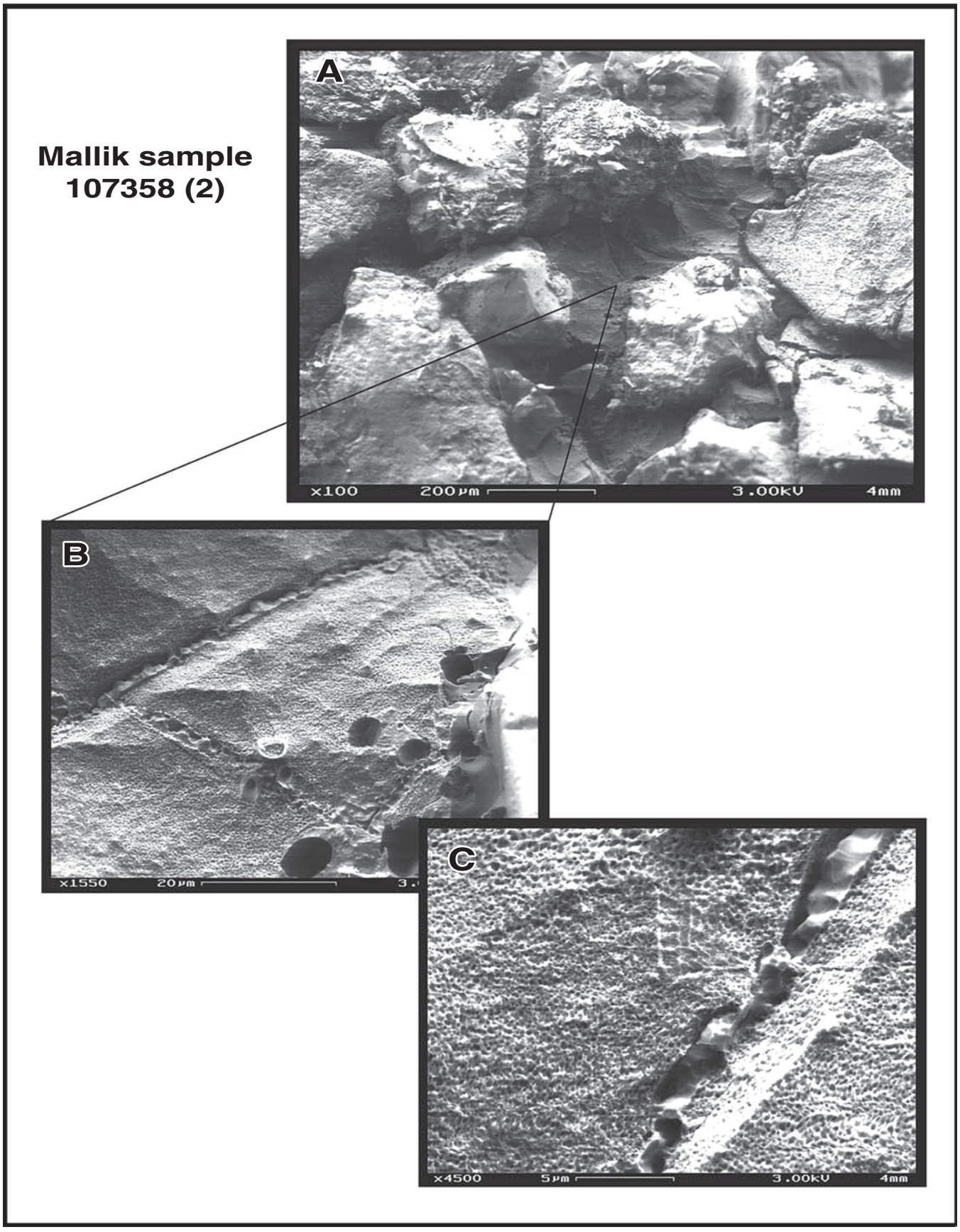
Mallik sample
107358 (2)
A
x100 200µm 3.00kV 4mm
B
x1550 20µm
C
x4500 5µm 3.00kV 4mm

Figure A4.

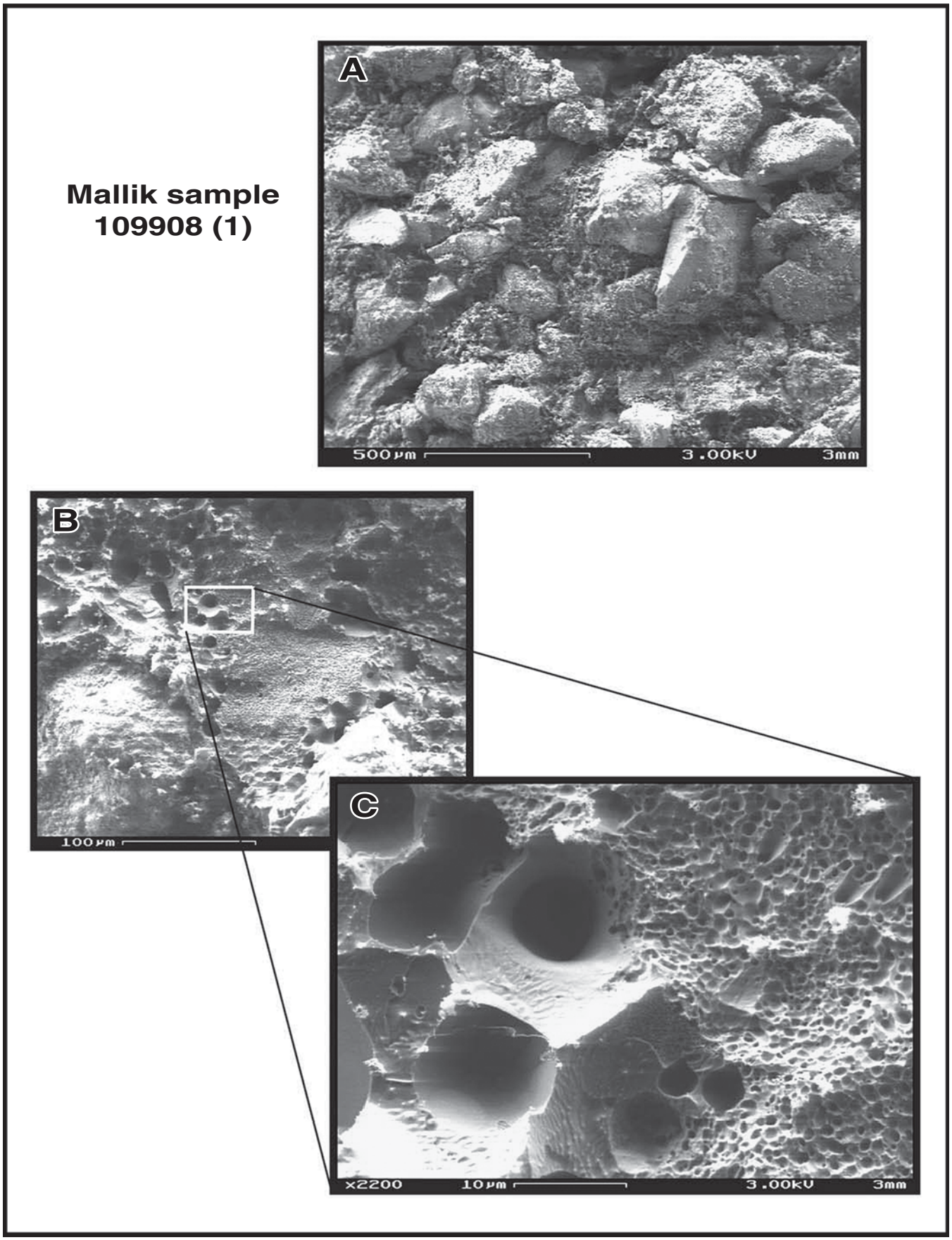
Mallik sample
109908 (1)
A
500 µm
3.00kV
3mm
B
100 µm
C
x2200
10 µm
3.00kV
3mm

Figure A5.

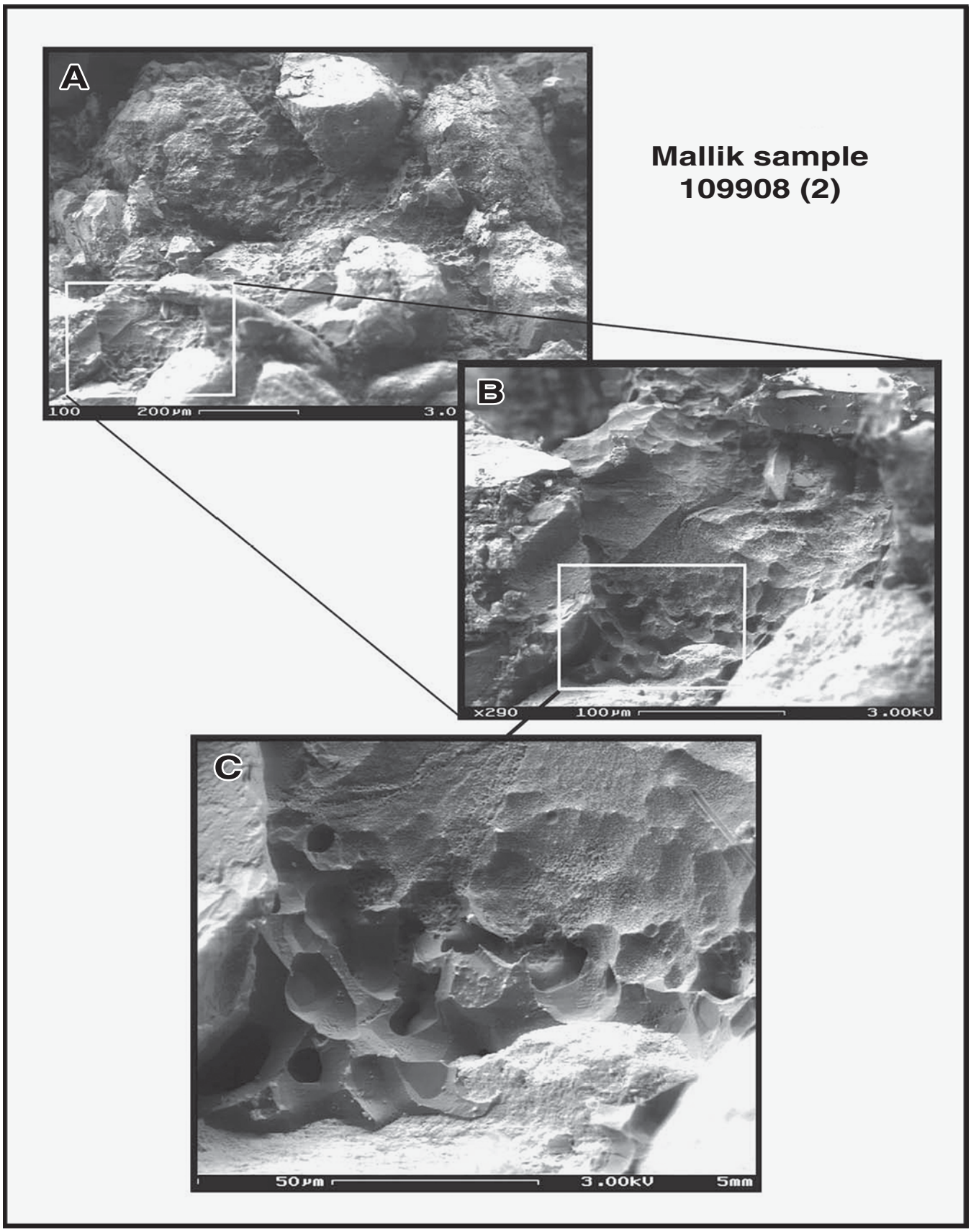
A
100
200 µm
3.0
Mallik sample
109908 (2)
B
x290
100 µm
3.00kV
C
50 µm
3.00kV
5mm

Figure A6.

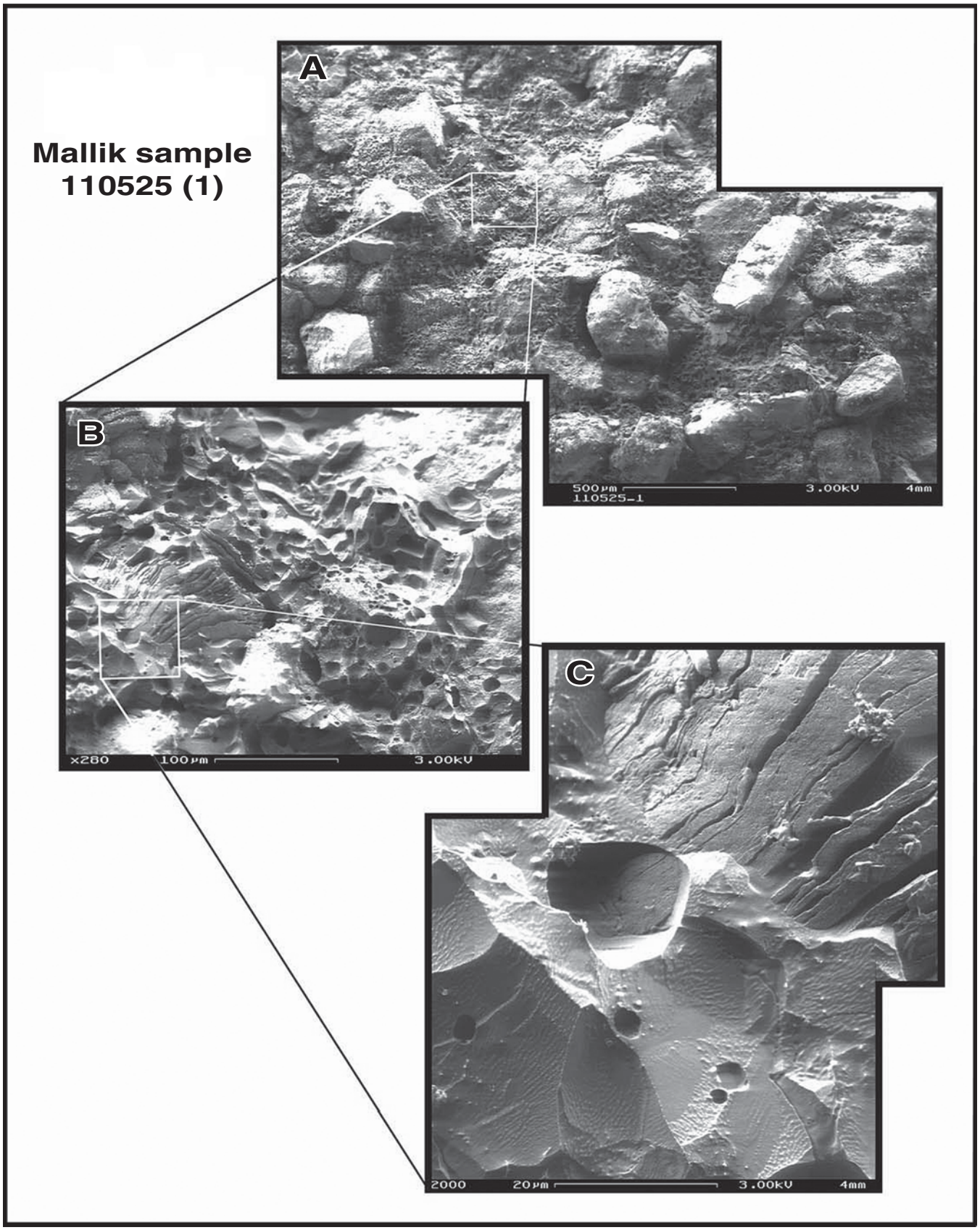
Mallik sample
110525 (1)
A
500 µm
110525-1
3.00kV
4mm
B
x280
100 µm
3.00kV
C
2000
20 µm
3.00kV
4mm

Figure A7.

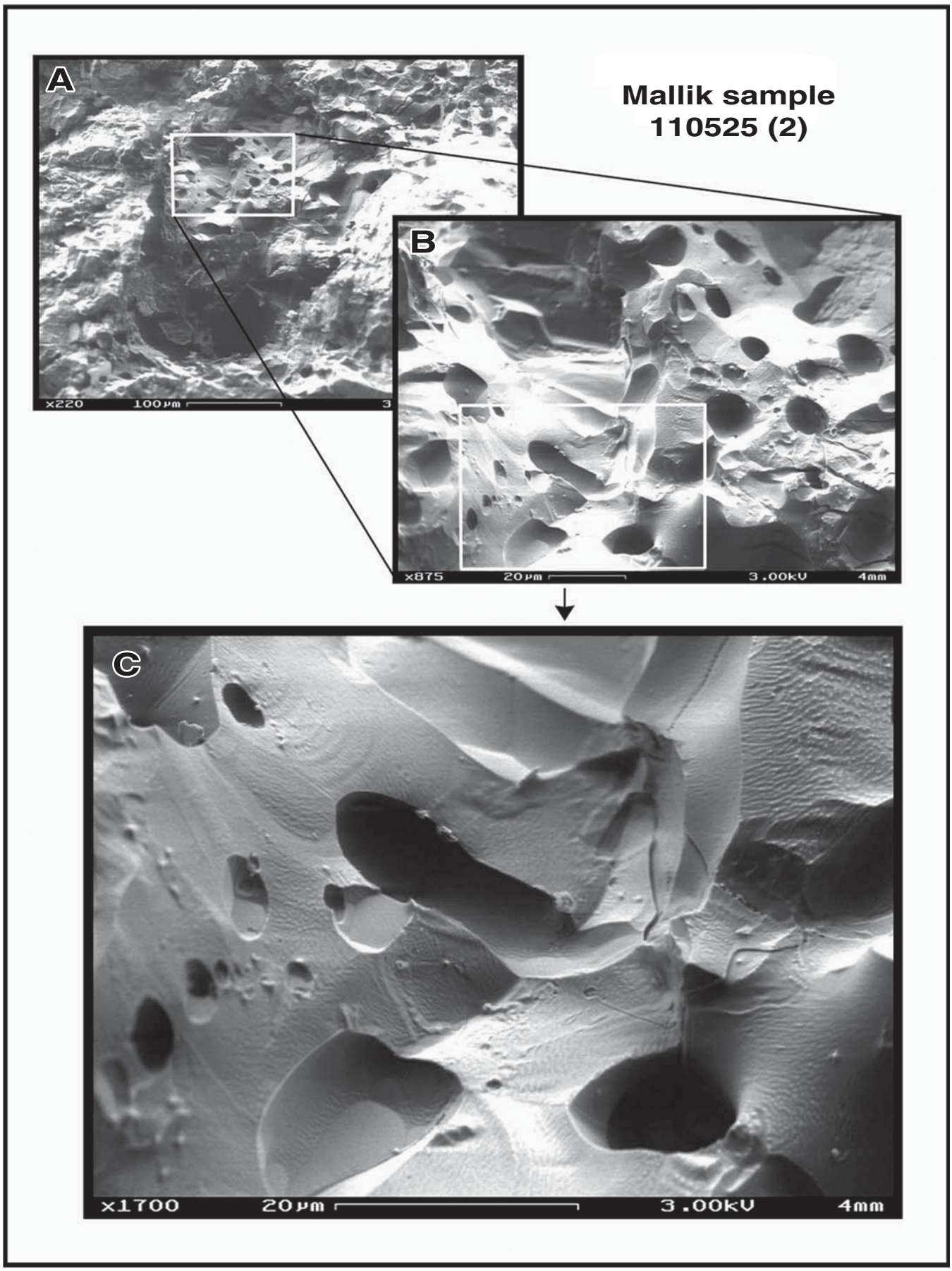
A
Mallik sample
110525 (2)
x220 100µm 3
B
x875 20µm 3.00kV 4mm
C
x1700 20µm 3.00kV 4mm

Figure A8.